FISEVIER

Contents lists available at ScienceDirect

Manufacturing Letters

journal homepage: www.elsevier.com/locate/mfglet



Letters

Transfer learning for predictive quality in laser-induced plasma micromachining



Mengfei Chen^a, Rajiv Malhotra^b, Weihong Guo^{a,*}

- ^aDepartment of Industrial and Systems Engineering, Rutgers University-New Brunswick, Piscataway, NI 08854, USA
- ^b Department of Mechanical and Aerospace Engineering, Rutgers University-New Brunswick, Piscataway, NJ 08854, USA

ARTICLE INFO

Article history: Received 16 May 2023 Received in revised form 25 July 2023 Accepted 20 August 2023 Available online 3 September 2023

Keywords:
Laser-induced plasma micro-machining
(LIPMM)
Transfer learning
Acoustic emission
Deep learning
Predictive quality

ABSTRACT

In laser-induced plasma micro-machining (LIPMM), a focused, ultrashort pulsed laser beam creates a highly localized plasma zone within a transparent liquid dielectric. When the beam intensity is greater than the breakdown threshold in the dielectric media, plasma is formed which is then used to ablate the workpiece. This paper aims to facilitate in-situ process monitoring and quality prediction for LIPMM by developing a deep learning model to (1) understand the relationship between acoustic emission data and quality of micro-machining with LIPMM, (2) transfer such understanding across different process parameters, and (3) predict quality accurately by fine-tuning models with a smaller dataset. Experiments and results show that the relationship learned from one process parameter can be transferred to other parameters, requiring lesser data and lesser computational time for training the model. We investigate the feasibility of transfer learning and compare the performance of various transfer learning models: different input features, different CNN structures, and the same structure with different fine-tuned layers. The findings provide insights into how to design effective transfer learning models for manufacturing applications.

© 2023 Society of Manufacturing Engineers (SME). Published by Elsevier Ltd. All rights reserved.

1. Introduction

Laser-induced plasma micro-machining (LIPMM) is a novel multi-material, tool-less process that removes material at the microscale by plasma-matter interaction [1–3]. Compared with conventional laser ablation, LIPMM overcomes the shortcomings in machining materials with low absorptivity or high reflectivity [2] and has been shown to machine metal alloys, transparent materials, brittle ceramics, and polymers [4,5]. In addition, LIPMM enables reduced heat-affected zone (HAZ), enhanced material removal rates, and higher aspect ratios of the machined features [6].

The quality of micro-machining with LIPMM, indicated by the uniformity in channel depth along the channel length, is acutely sensitive to laser parameters such as pulse energy, pulse frequency, and laser speed [7]. The quality of the micro-machined workpiece is also affected by the generation of bubbles and ablation debris [8]. Specifically, bubble-induced quality deterioration is a well-known issue [9]. In order to achieve desired quality, it is necessary to develop methods that facilitate in-situ process monitoring and

quality prediction for LIPMM. This paper aims to fill in two gaps in literature. First, there is no work reported on the in-situ monitoring or predictive quality analysis for LIPMM, because LIPMM is a newly developed process still under exploration. Second, none of the existing works has investigated models that can be generalized to a variety of process parameters.

Looking into similar processes, there have been analytical, numerical-based, or AI-based methods developed for process monitoring or quality prediction in laser beam machining. Although some of those methods can be applied to LIPMM, they focus on finding the best combination of process parameters, rather than in-situ monitoring or quality prediction. Moreover, most existing works only use laser parameters (e.g., pulse energy) as the input for quality prediction, while in-situ sensing data might help to improve prediction accuracy by capturing uncertainties in the actual process. In addition, none of the existing works has investigated models that can be generalized in a variety of process parameters (e.g., different laser parameters and a variety of materials). Besides, there is no in-situ monitoring for the LIPMM process reported. To fill in these gaps, this paper develops a transferable method for in-situ monitoring and quality prediction in LIPMM considering a variety of process parameters.

E-mail address: wg152@soe.rutgers.edu (W. Guo).

^{*} Corresponding author.

The objective of this paper is to develop a transferrable method for in-situ process monitoring and quality prediction in LIPMM. This study aims to provide the following contributions to the state-of-the-art: firstly, deep CNN and process parameter-informed (para-informed) deep CNN models are proposed for understanding the relationship between acoustic emission data and quality of micro-machining with LIPMM; secondly, such understanding is transferred across different process parameters by transfer learning and fine-tuning models with a smaller dataset; thirdly, the feasibility of transfer learning is investigated and compared under different designs of CNN architecture and input features; lastly, the performance of transfer learning with different designs of fine-tuning strategies are compared to provide insights on how to design effective transfer learning models.

2. Sensing and data collection

LIPMM experiments were performed with a Quantum Light Instruments pulsed laser (3 ns pulse duration, 50 mJ pulse energy at a wavelength of 526 nm). The 4 mm diameter laser beam was optically reduced to a 120 µm diameter beam at the focal point. The workpiece material was 6061 Aluminum purchased from McMaster Carr. Deionized water was used as the dielectric liquid. The workpiece was kept in a glass beaker with a 2 mm thick water layer above it. The glass beaker was, in turn, kept on a motorized XYZ stage that had a resolution of 50 nm. The focal point for LIPMM was identified by creating holes at different vertical distances of the lens from the workpiece and examining the depth of the machined features. As in past work on LIPMM, the focal point chosen was that at which the machined depth was maximum and after which the machined depth decreased again. Microchannels were machined by moving the laser at a specified laser speed and pulse energy along the desired direction in a single pass, i.e., without translating the laser spot in the vertical direction. The dimensions of the machined channels and holes were measured using a Keyence optical profilometer. An omnidirectional hydrophone (Aguarian hydrophones, model AS-1) with a 1 Hz to 100 kHz range and a sensitivity of 40 μ V/Pa was kept at a fixed distance from the focal spot during machining, and it was connected to a LabView device to record the acoustic signals during LIPMM. The criteria for assigning good or bad labels were based on the uniformity of machining from the observed morphology of the machined channels. Different combinations of the laser speed, laser pulse frequency, and laser pulse energy resulted in good-quality and bad-quality (with defects) micro-machined workpieces. Since this paper focuses on in-situ sensing/monitoring rather than delineating process effects, the parametric effects on defects are not discussed in this paper.

Examples of the micro-machined workpiece are shown in Fig. 1. The Fig. 1(a) samples were labeled as bad; Fig. 1(b) samples were labeled as good based on observably uniform depth along the microchannel's length. Fig. 1(c) shows the raw AE signal from one of the experiments. The x-axis is time, and the y-axis is voltage, which is linearly proportional to the actual acoustic pressure via a known constant multiplication factor. We segment the data series into smaller segments to alleviate the training burden. In addition, segmenting data helps to enlarge the sample size, leading to a good number of segments to have the models properly trained. Furthermore, when segmenting the AE signal in time order we can correlate each segment to a quality prediction. This enables us to locate problematic segments for further root cause analysis. Therefore, we cut each AE data series into equal-length, non-overlapping segments. The length of the segment is based on the laser pulse period. Fig. 1(d) and (e) show the first and second segments from the raw signal in Fig. 1(c). The segments have the same length and similar waveform-constant patterns.

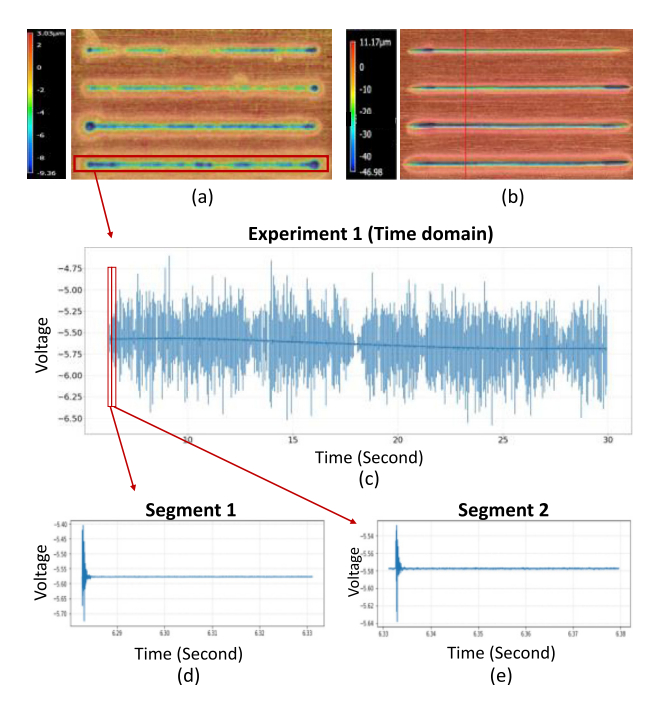


Fig. 1. Examples from LIPMM: (a) bad machining; (b) good machining; (c) the raw AE signal from one of the LIPMM experiments; (d) the first segment from the AE signal; (e) the second segment from the AE signal.

3. Method

3.1. Deep convolutional neural network (CNN) for AE signal and LIPMM quality

The overall framework of the proposed method is illustrated in Fig. 2. AE signals are cut into non-overlapping segments $\mathbf{s}_1, \mathbf{s}_2, \cdots, \mathbf{s}_N \in \mathbb{R}^{n_p \times 1}$ according to the pulse period, where N is the total number of segments and n_n is the length of the pulse period. Depending on how AE segments are analyzed as input, three types of models are developed for comparison, namely, FFTNet, Wave-Net, and AcouNet. AE segments can be converted from the time domain into the frequency domain using Fast Fourier Transform (FFT), and a CNN named FFTNet is proposed to predict quality using frequency features computed by FFT. Selected frequency features $m{f}_1, m{f}_2, \cdots, m{f}_N \in \mathbb{R}^{n_f imes 1}$ are fed into a CNN, where n_f is the number of selected features. Decomposing signals with Discrete Wavelet Transform (DWT) allows us to obtain low frequency signals and high frequency signals at each level of decomposition. Selected wavelet features $\mathbf{w}_1, \mathbf{w}_2, \cdots, \mathbf{w}_N \in \mathbb{R}^{n_f \times 1}$ are fed into a CNN. In AcouNet, the AE segments are used directly as input into a CNN. Different architectures of AcouNet are proposed for comparison. The performance among models with different finetuning strategies are also compared in AcouNet. To enhance models' ability in handling more complex tasks, the FFTNet, WaveNet, and AcouNet models are extended by adding process parameters to the input information, forming process parameter-informed (para-informed) CNNs.

Convolutional neural networks are well suited for processing acoustic signal [10]. In each of the proposed models, the input is processed by a series of one-dimensional convolutional layers with ReLU activation functions and then pooling layers, followed by a fully connected layer and several hidden layers. The output is a 2×1 vector indicating the label of micro-machining quality (vector [1, 0] for bad and [0, 1] for good). As shown in Fig. 2, five CNNs are developed, and their names include the number of convolu-

Models: Transfer Learning with Different Models and Tuning Layers

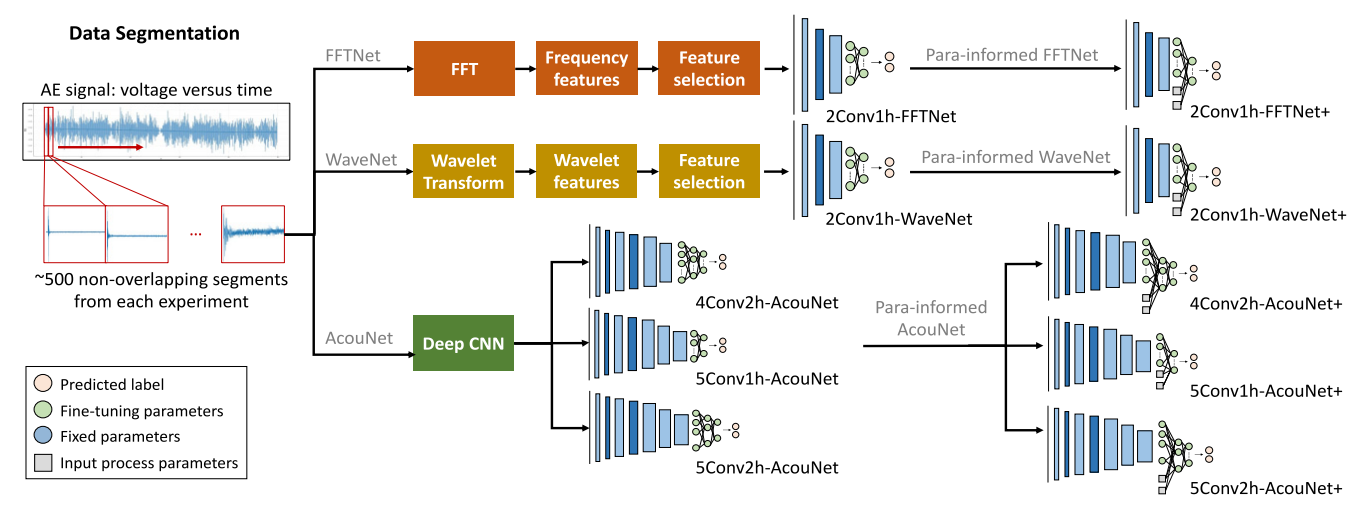


Fig. 2. Overall framework of the proposed method.

tional layers, the number of hidden layers, and the type of input used (FFTNet or WaveNet or AcouNet). To prevent overfitting, we also add a 0.2 dropout rate to the fully connected and hidden layers, which means that each neuron on these layers will be discarded with 0.2 probability.

3.2. Transfer learning with deep CNN

Transfer learning is a paradigm in which a model that has already been trained on a similar task is reused to complete a second task with minimal training cost. Fig. 3 illustrates different finetuning strategies based on 4Conv2h-AcouNet for comparison. Fig. 3 (a) shows that all convolutional layers are fixed, and all fully connected layer and hidden layers are used for fine-tuning, called fc-h2. In Fig. 3(b), all convolutional layers and the fully connected layer are fixed, and the last two hidden layers are used as finetuning layers, called h1-h2. Fig. 3(c) shows that the last convolutional layer (Conv4) is added to the fine-tuning layers, called Conv4-h2. Fig. 3(d) provides an example of the *para*-informed model, named 4Cov2h-AcouNet+. Two gray boxes refer to two neurons representing pulse energy and laser speed, respectively.

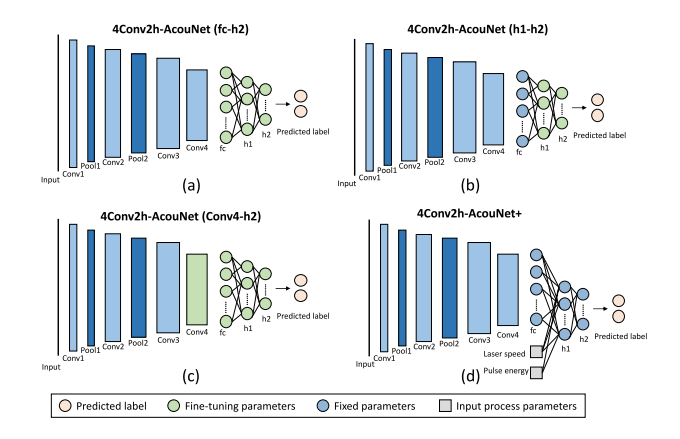


Fig. 3. Different fine-tuning layers designed in this paper: (a) 4Conv2h-AcouNet with fine-tuning layers fc, h1, and h2; (b) 4Conv2h-AcouNet with fine-tuning layers h1 and h2; (c) 4Conv2h-AcouNet with fine-tuning layers Conv4, fc, h1, and h2; (d) architecture of a para-informed CNN model "4Conv2h-AcouNet+".

4. Case study

We apply the proposed models in two transfer learning tasks. In Task-1, we develop the CNN models using data from process parameter Para-1 and then transfer the models to Para-2. Experimental data from Para-1 are used to train the base CNN models. A small amount of data from Para-2 is used for updating weights in fine-tuning layers. Total 1883 AE segments (1004 for bad, 879 for good) are used for obtaining the weights in the base model, and 726 AE segments (363 for bad, 363 for good) are used for updating the weights in fine-tuning layers in transfer learning. In Task-2, we further transfer the CNN models trained from Para-1 to three additional process parameters Para-3, Para-4, and Para-5. Experimental data of Para-1 are used for training the parainformed CNN models. Similarly, a total of 1883 AE segments (1004 for bad, 879 for good) are used for obtaining the weights in the base model, and a total of 612 AE segments (306 for bad, 306 for good) are used for updating the weights in fine-tuning layers in transfer learning. For both tasks, 80% of the data are used for training and 20% are reserved for testing. In our experiment, the length of the pulse period is around 1700, so we set segment length $n_p = 1700$. For FFTNet and WaveNet, features are selected based on the linear correlation importance score. There is a trade-off in determining the number of selected features n_f : a large n_f may bring more information to the CNN model but may also lead to redundant features and add to training burden, while a small n_f may cause information loss. Therefore, we select features with importance score higher than 0.02, and $n_f = 120$. In training the models, we use the cross-entropy loss function and select the stochastic gradient descent method as the optimizer.

Table 1(a) shows the transfer learning performance for different CNN models in Task-1, including the accuracy $\left(\frac{TP+TN}{TP+FP+TN+FN}\right)$, precision $\left(\frac{TP}{TP+FP}\right)$, negative predictive value $\left(NPV=\frac{TN}{TN+FN}\right)$, sensitivity $\left(\frac{TP}{TP+FN}\right)$, and specificity $\left(\frac{TN}{FP+TN}\right)$.

In this study, the "bad" class is positive and "good" is negative; TP (true positive) refers to the correct prediction of undesired quality, TN (true negative) refers to the correct identification of satisfying quality, and FP (false positive) and FN (false negative) are the errors in prediction.

Comparing the AcouNet models in Table 1(a) reveals how the number of deep convolutional layers affects the learning and prediction performance. Transfer learning drastically reduces training

Table 1Transfer learning performance comparison.

(a) Transfer lea	arning performar	nce comparis	on of differe	ent mode	els on Para-2	data (Task-1)	•		
Model name	Fine-tuning layers	Accuracy	Precision	NPV	Sensitivity	Specificity	Training time on transfer layers (hr)	Training time on base model (hr)	Base model accuracy
4Conv2h- AcouNet	fc-h2	0.9448	0.8760	0.9941	0.9180	0.9907	6.79	35,22	0.9766
	h1-h2	0.8993	0.7694	1.0000	0.8484	1.0000	6.03	35.22	
	Conv4-h2	0.9469	0.9497	0.9450	0.9626	0.9264	7.72	35.22	
5Conv1h- AcouNet	fc-h1	0.9682	0.9935	0.9509	0.9325	0.9953	6.03	42.25	0.9824
5Conv2h- AcouNet	fc-h2	0.9708	0.9872	0.9593	0.9448	0.9907	7.83	43.22	0.9824
2Conv1h- FFTNet	fc-h1	0.6499	0.9445	0.6228	0.773	0.972	4.19	15.78	0.7966
2Conv1h- WaveNet	fc-h1	0.9549	0.9563	0.9539	0.9563	0.9673	4.19	15.78	0.9771
(b) Transfer le	arning performa	nce comparis	on of differe	ent mode	els on Para-3,	Para-4, and I	Para-5 data (Task-2).		
Model name	Fine-tuning layers	Accuracy	Precision	NPV	Sensitivity	Specificity	Training time on transfer layers (hr)	Training time on base model (hr)	Base model accuracy
4Conv2h-	fc-h2	0.9390	0.9000	1	1	0.8648	6.54	35.22	0.9618
AcouNet+	h1-h2	0.8170	0.7500	1	1	0.5945	6.16	35.22	
	Conv4-h2	0.9390	0.9000	1	1	0.8648	7.89	35.22	
5Conv1h- AcouNet+	fc-h1	0.8536	0.7894	1	1	0.6756	6.16	42.25	0.9670
5Conv2h- AcouNet+	fc-h2	0.8902	0.8333	1	1	0.7567	8.01	43.22	0.9670
2Conv1h- FFTNet+	fc-h1	0.6951	0.6428	1	1	0.3243	4.28	15.78	0.8029
2Conv1h-	fc-h1	1.0000	1.0000	1	1	1.0000	4.28	15.78	1.0000

time, as evidenced by a 4Conv2h-AcouNet model's training time reduction from 35.22 to 6.79 h, achieving 94.48% accuracy. Accuracy and learning speed are influenced by the number of finetuning layers: fewer layers save time at the potential cost of accuracy, and vice versa. For instance, fine-tuning Conv4-h2 layers led to marginally better accuracy (94.69%) but required additional 0.93 h. Deeper convolutional layers enhance learning performance, with models 5Conv1h-AcouNet and 5Conv2h-AcouNet outperforming the 4Conv2h-AcouNet model, achieving 96.82% and 97.08% accuracies, respectively. Input features significantly affect model performance, with the 2Conv1h-WaveNet model outperforming the 2Conv1h-FFTNet model (95.49% versus 64.99% accuracy), proving wavelet features' effectiveness in LIPMM quality prediction. Table 1(b) shows the transfer learning performance for para-informed CNN models in Task-2. In fine-tuning the 4Conv2h-AcouNet+ model, both Conv4-h2 and fc-h2 strategies achieve 93.90% accuracy, suggesting the Conv4 layer redundant for additional fine-tuning. The 5Conv2h-AcouNet+ model outshines the 5Conv1h-AcouNet+ with 89.02% accuracy, albeit at a longer training time (8.01 versus 6.16 h). This showcases the trade-off between more in-depth information capture and increased training time. In contrast, the 2Conv1h-FFTNet+ model, using only frequency features, attains a poor accuracy (69.51%), highlighting the crucial role of wavelet features in quality prediction demonstrated by the 2Conv1h-WaveNet+ model's 100% accuracy. A comparison of the base models reveals the advantage of an additional convolutional layer in the 5Conv2h-AcouNet model, which outperforms the 4Conv2h-AcouNet model. Despite transfer learning models showing a minor accuracy drop, their performance remains robust, verifying their feature extraction and analysis potential.

5. Conclusion

Capturing acoustic emission during the laser-induced plasma micro-machining process provides opportunities for in-situ process monitoring and quality prediction. We develop deep learning models that can timely and accurately predict the quality of micromachining in LIPMM process. The models learn the relationship between acoustic emission data and quality of micro-machined workpiece with LIPMM. The relationship learned from one process setting can be transferred to other process parameters, requiring less data and less computational time. Results show that transfer learning is feasible and effective in predicting LIPMM quality.

Declaration of Competing Interest

The authors declare that they have no known competing financial interests or personal relationships that could have appeared to influence the work reported in this paper.

Acknowledgement

This work was supported by the National Science Foundation, USA, grant CMMI # 2001081.

References

- Pallav K, Ehmann KF. Feasibility of laser induced plasma micro-machining (LIP-MM). In: International Precision Assembly Seminar. Springer; 2010. p. 73–80.
- [2] Pallav K, Saxena I, Ehmann K. Laser-induced plasma micromachining process: principles and performance. J Micro Nano-Manuf 2015;3(3).
- [3] Zhang Y, Bhandari S, Xie J, Zhang G, Zhang Z, Ehmann K. Investigation on the evolution and distribution of plasma in magnetic field assisted laser-induced plasma micro-machining. J Manuf Process 2021;71:197–211.
- [4] Malhotra R, Saxena I, Ehmann K, Cao J. Laser-induced plasma micro-machining (LIPMM) for enhanced productivity and flexibility in laser-based micromachining processes. CIRP Ann 2013;62(1):211–4.
- [5] Saxena I, Ehmann KF. Multimaterial capability of laser induced plasma micromachining. J Micro Nano-Manuf 2014;2(3).
- [6] Saxena I, Ehmann K, Cao J. High throughput microfabrication using laser induced plasma in saline aqueous medium. J Mater Process Technol 2015;217:77–87.
- [7] Bakhtiyari AN, Wang Z, Wang L, Zheng H. A review on applications of artificial intelligence in modeling and optimization of laser beam machining. Opt Laser Technol 2021;135:106721.

- [8] Pallav K, Saxena I, Ehmann KF. Comparative assessment of the laser-induced plasma micromachining and the ultrashort pulsed laser ablation processes. J Micro Nano-Manuf 2014;2(3).
- [9] Zhang Z, Zhang Y, Liu D, Zhang Y, Zhao J, Zhang G. Bubble behavior and its effect on surface integrity in laser-induced plasma micro-machining silicon wafer. J Manuf Sci Eng 2022;144(9):091008.
 [10] Aytar Y, Vondrick C, Torralba A. Soundnet: Learning sound representations from unlabeled video. Adv Neural Inf Proces Syst 2016;29.